Experiment and Computation on Aerodynamic Characteristics and Flow Visualisation of Basic Airfoils at Very-Low Reynolds Numbers

Takahashi, Erika
Department of Mechanical Engineering, Doshisha University

Onishi, Kazuki
Department of Mechanical Engineering, Doshisha University

Tanigawa, Hirochika
Department of Mechanical Engineering, NIT, Maizuru College

Uchida, Takanori
Research Institute for Applied Mechanics, Kyushu University

他

EXPERIMENT AND COMPUTATION ON AERODYNAMIC CHARACTERISTICS AND FLOW VISUALIZATION OF BASIC AIRFOILS AT VERY-LOW REYNOLDS NUMBERS

E. TAKAHASHI[1], K. ONISHI[1], H. TANIGAWA[2], K. UCHIDA[3], K. SUGITANI[3] and K. HIRATA[1]
[1] Department of Mechanical Engineering, Doshisha University
Tataramiyakodani 1-3, Kyotanabe, Kyoto 610-0321, Japan

[2] Department of Mechanical Engineering, NIT, Maizuru Collage
Shiroya 234, Maizuru, Kyoto 625-0016, Japan

[3] RIAM, Kyushu University
Kasuga 6-1, Fukuoka 816-8580, Japan

ABSTRACT

We have been requiring more precise knowledge about the aerodynamic characteristics of airfoils especially in a low-Reynolds-number range less than 10^6, because of the recent miniaturisation of robots such as unmanned aerial vehicles known as UAVs or micro air vehicles known as MAVs, in addition to the importance of insect/bird flight dynamics, small-scale machines like micro fluid machineries and micro combustion engines and so on. In the present studys we investigate the relationship between various aerodynamic characteristics and attack angle α for FP (a flat plate), NACA0015 and iNACA0015 (the NACA0015 placed back to front) by numerical analysis and water-tank experiment at $Re = 1.0\times10^2 - 8.0\times10^2$. Then, we reveal the effects of α upon various aerodynamic characteristics such as the lift coefficient C_L, drag coefficient C_D and the lift-to-drag ratio C_L/C_D. In order to discuss the revealed α effects, we further visualise the flow around the airfoils using the Q value, helicity and streamlines at $\alpha = 0 - 24$ deg., together with PIV analysis based on water-tank experiment. Such results suggest that FP is similar not with NACA0015 but with iNACA0015 from an aerodynamic point of view.

INTRODUCTION

The airfoil is one of the most elemental devices for flying/swimming robots to control flow and its reacting force, which determines robots' basic performances. However, the aerodynamic characteristics of the airfoil have been researched mainly in a high Reynolds-number range more than 10^6, in a historic context closely related with the developments of airplanes and high-speed fluid machineries in the last century.[(1) - (4)]

On the other hand, we have been requiring more precise knowledge about the aerodynamic characteristics of the airfoil especially in a low Reynolds-number range less than 10^6, because of the recent miniaturisation of robots such as unmanned aerial vehicles known as UAVs or micro air vehicles known as MAVs[(5), (6)], in addition to the importance of insect/bird flight dynamics, small-scale machines like micro fluid machineries and micro combustion engines and so on.

Concerning the aerodynamic characteristics at low Reynolds numbers, there have been several studies[(7) - (26)]. However, in such a low Reynolds number range, our knowledge has not been enough yet, due to the laminar-to-turbulent transition with strong nonlinearity which brings us some technical difficulties in the accuracies of analyses, computations and experiments.

In the present study, we investigate the relationship between various aerodynamic characteristics and attack angle α for a flat plate, NACA0015 and iNACA0015 (the NACA0015 placed back to front) by numerical analyses and water-tank experiments at $Re = 1.0\times10^2 - 8.0\times10^2$.

METHOD

Models

Figure 1 shows the present models. They are three kinds of two-dimensional airfoils, namely, a flat plate (hereinafter, refered to as FP), NACA0015 as a typical high-performance airfoil at high Re and iNACA0015 which is the NACA0015 placed back to front.

Computational procedure

In many actual situations, most of the flow at $Re < 10^6$ could be usually regarded as incompressible. So, we suppose the incompressible full Navier-Stokes equations in three dimensions. We approximately solve the equations by a finite-difference method using the MAC scheme as velocity-and-pressure coupling, a third-order-upwind difference scheme in spatial discretisation of convective terms, a second-order-central difference scheme in spatial discretisation of the other terms and the Euler explicit scheme in a time marching.

As a spatial grid, we use a staggered grid as shown in Fig. 2, which is a boundary-fitted one with a generalised coordinate system (ξ, η). Here, ξ and η represent a tangential and normal coordinates with respect to the airfoil surface, respectively. The boundary condition on the airfoil surface is viscid. On the outer boundaries of the computational domain, we suppose the Dirichlet condition as $u = 1$, $v = 0$ and $w = 0$. Span s of both model and grid in the z direction is usually equal to the chord c. And, we suppose the periodic boundary condition at both the end of span. We proceed with the time-manching computations, during which we monitor both the values of C_D and C_L, to judge whether the total computation time is enough or not for fully-saturated conditions.

Experimental procedure

The present experimental apparatus consists of a water tank, a model (a cylinder with an airfoil cross section), a bogie, a slide projector and a camera. We carry out flow visualization around the model. The model is attached to the towing bogie which horizontally moves at a constant speed. In the present experiment, we examine only FP.

Visualised planes are both (1) the plane perpendicular to the model and (2) the plane perpendicular to the mainstream. And in the present report, we will show the former. Figure 3 shows the experimental apparatus for the former, namely the flow visualization on an airfoil's cross-section plane.

RESULTS AND DISCUSSION

Velocity vectors obtained by experiment

Figs. 4 – 6 show the PIV-analysed images which are created from the movies taken in experiment for FP. All the images are flow-velocity vectors on a plane perpendicular to the model's axis at its centre span. Figs. 4, 5 and 6 indicate at Re = 1.0×10^2, 4.0×10^2 and 8.0×10^2, respectively. In panels (a) and (b) in each figure are at α = 4 deg. and 24 deg., respectively. The magnitude of flow-velocity vector corresponds to the vector's length, and a legend is shown on the right side of each panel.

The following facts can be seen from these figures. First of all, at all Re's, when α = 4 deg., the flow around the airfoil is almost uniform. That is, flow separation does not occur within the range of $Re \le 8.0\times10^2$ at $\alpha \le 4$ deg. for FP. Next, when α = 24 deg., the wake of the airfoil is far from uniform at all Re's. More specifically, flow separation occurs near the leading edge of the airfoil, and it often, but not always, leads to the transition to the unsteady flow where the separated shear layer is cyclically formed into vortices traveling downstream above the airfoil. In the present study, flow is always unsteady at all Re's atα = 24 deg. So, we should note that the flow at α = 24 deg. depends upon time. And such instantaneous images as Figs. 4(b), 5(b) and 6(b) are affected by time.

Velocity vectors obtained by computation

Figs. 7 – 9 show the velocity vectors obtained by computation, as well as Figs. 4 – 6 by experiment. All the images are flow-velocity vectors on a plane perpendicular to the model's axis at its centre span. Figs. 7, 8 and 9 indicate at Re = 1.0×10^2, 4.0×10^2 and 8.0×10^2, respectively. In panels (a) and (b) in each figure are at α = 4 deg. and 24 deg., respectively. The magnitude of flow-velocity vector corresponds to the vector's length, and a legend is shown on the right side of each panel. The colour of each velocity vectors denotes the value of x-component velocity u as shown by the legend on the upper left hand.

The following facts can be seen from these figures. First of all, at all Re's, when α = 4 deg., the flow around the airfoil is almost uniform. That is, flow separation does not occur within the range of $Re \le 8.0\times10^2$ at $\alpha \le 4$ deg. for FP. Next, when α = 24 deg., the wake of the airfoil is far from uniform at all Re's. More specifically, flow separation occurs near the leading edge of the airfoil, and it often, but not always, leads to the transition to the unsteady flow where the separated shear layer is cyclically formed into vortices traveling downstream above the airfoil. In the present study, flow is always unsteady at all Re's atα = 24 deg. So, we should note that the flow at α = 24 deg. depends upon time. And such instantaneous images as Figs. 4(b), 5(b) and 6(b) are affected by time.

Comparison between experiment and computation

Comparing such experiments as Figs. 4 – 6 with such computations as Figs. 7 – 9, you can find many similarities. One of the similarities is in spatial structure of flow. Specifically speaking in both the experiment and the computation, the flow at α = 4 deg. is almost uniform. On the other hand, α = 24 deg., there always exist the flow separation at a leading edge, the cyclical vortex formations from the separated shear layer, and the downstream traveling of the formed vortices. Then, the experiment and the computation well coincide each other, qualitatively and consistently.

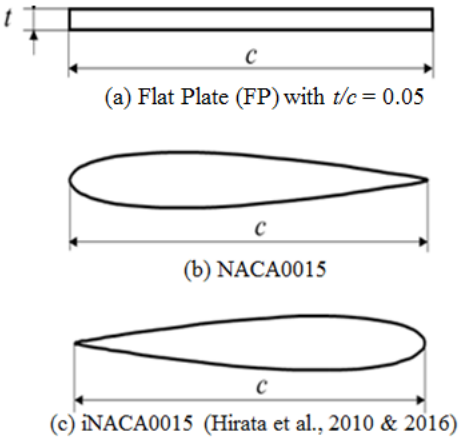

Figure 1. Models: two-dimensional airfoils.

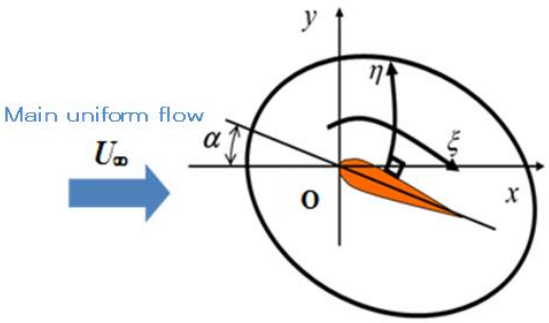

Figure 2. Coordinate system for computational grid.

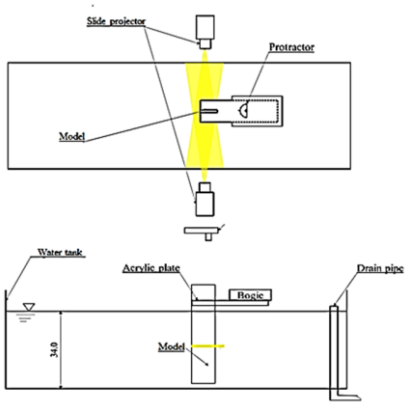

Figure 3. Experimental apparatus for flow visualization on an airfoil's cross-section plane.

Aerodynamic characteristics at $Re = 1.0\times10^2$

Fig. 10 shows one of the aerodynamic characteristics; namely, the lift-to-drag ration the relationship of C_L/C_D with respect to the angle of attack α for three kinds of airfoils at $Re = 1.0\times10^2$.

For all the airfoils, we can see that C_L/C_D increases, as α increases from zero. The increase is not monotonical, but ceases at $\alpha \approx 4$ deg. And at $\alpha \geq 4$ deg., C_L/C_D decreases with increasing α inreverse. From practical viewpoint, FP is the most excellent at $Re = 1.0\times10^2$ due to the large C_L/C_D. In addition, If we compare with the present results with Taira et al. [21] and Sun & Boyd [15] , we can confirm qualitative and quantitative agreement.

Aerodynamic characteristics at $Re = 4.0\times10^2$

Fig. 11 shows the relationship of C_L/C_D with respect to α of the three kinds of airfoils at $Re = 4.0\times10^2$. For both FP and iNACA0015, a clear peak of C_L/C_D appears at $\alpha \approx 10$ deg. In contrast, for NACA0015, C_L/C_D monotonically and gradually increases with increasing α at $\alpha \leq 20$ deg. And, C_L/C_D decreases an $\alpha \geq 20$ deg. Then, C_L/C_D attains the maximum at $\alpha \approx 20$ deg. From a practical point of view, FP is the most excellent at $Re = 1.0\times10^2$ due to the large C_L/C_D.

Aerodynamic characteristics at $Re = 8.0\times10^2$

Fig. 12 shows the relationship of C_L/C_D with respect to α of the three kinds of wings at $Re = 8.0\times10^2$. For both FP and iNACA0015, a peak of C_L/C_D appears at $\alpha \approx 10$ deg. In contrast, in NACA0015, it gradually increases by $\alpha \leq 20$ deg.

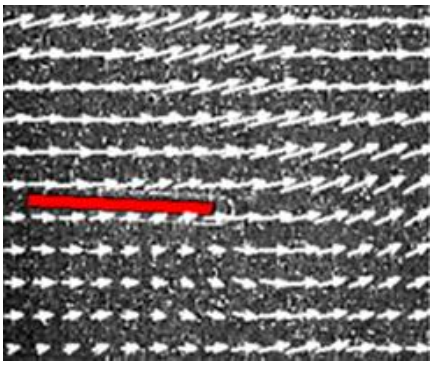

(a) At α = 4 deg. $1.0U_\infty$

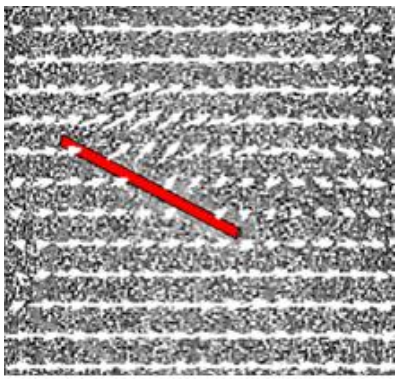

(b) At α = 24 deg. $1.0U_\infty$

Figure 4. Velocity vectors for FP at $Re = 1.0\times10^2$ by experiment.

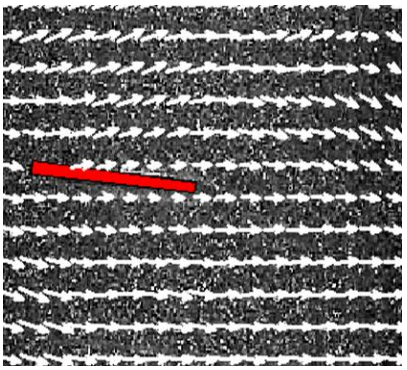

(a) At α = 4 deg. $1.0U_\infty$

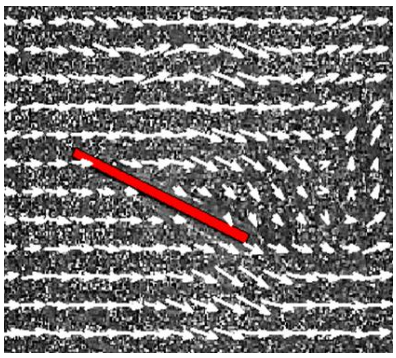

(b) At α = 24 deg. $1.0U_\infty$

Figure 5. Velocity vectors for FP at $Re = 4.0\times10^2$ by experiment.

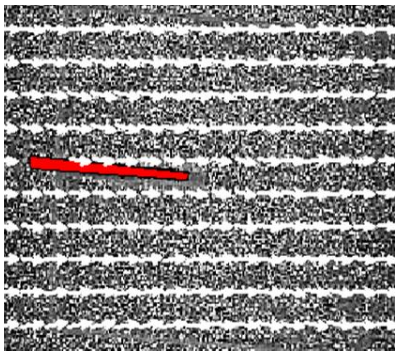

(a)At α = 4 deg. $1.0U_\infty$

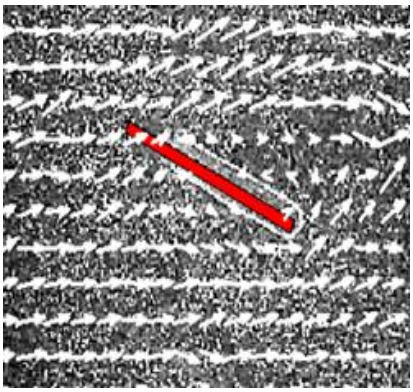

(b) At α = 24 deg. $1.0U_\infty$

Figure 6. Velocity vectors for FP at $Re = 8.0\times10^2$ by experiment.

And decreases with $\alpha \geq 20$ deg. In addition, peaks for FP is smaller than that for iNACA0015. Moreover, it can be seen that at $Re = 8.0\times10^2$, sharp leading edges of airfoil cause large peak's value of C_L/C_D. From a practical point of view, we can conclude that FP is superior due to large C_L/C_D in such a low Re region. On the other hand, NACA0015 shows superior aerodynamic characteristics on controllability with small stall feature to other two airfoils, although C_L/C_D is not large.

Classification of flow

Fig. 13 shows the velocity vectors at $Re = 8.0\times10^2$ and $\alpha = 10$ deg. for FP obtained by computation. From this figure and Fig. 9, the following can be seen. At $Re = 8.0\times10^2$ and $\alpha \leq 4$ deg., that is steady, and at $Re = 8.0\times10^2$ and $\alpha \geq 4$ deg., flow becomes unsteady.

Fig. 14 shows perspective views of flow around the FP at $Re = 8.0\times10^2$. More specifically, they are isosurfaces with $QC^2/U_\infty{}^2 = 3.0$, on which the colour of the surfaces denotes the value of relative helicity H_R as shown by the legend on the upper right hand.Panels (a), (b) and (c) are at α = 4 deg., 10 deg. and 24 deg., respectively.

At $\alpha = 4$ deg. and 10 deg., Q is uniform span wise. This uniformity suggests a two-dimensionality of flow. On the other hand, at $\alpha = 24$ deg., the Q is not uniform span wise. Then, flow is three-dimension.

From the above, we classify flow into three groups; namely, (1) steady and two dimensional, (2) unsteady (periodic) and two dimensional, (3) unsteady and three dimensional (periodic with random noise).

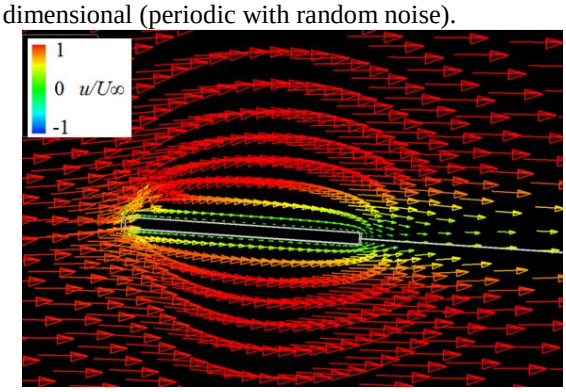

(a) At $\alpha = 4$ deg. $1.0U_\infty$

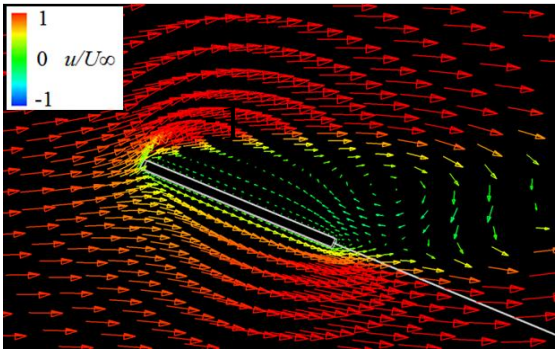

(b) At $\alpha = 24$ deg. $1.0U_\infty$

Figure 7. Velocity vectors for FP with $s/c = 1.0$ at $Re = 1.0\times10^2$ by computation. The colour of each velocity vectors denotes the value of x-component velocity u as shown by the legend on the upper left hand.

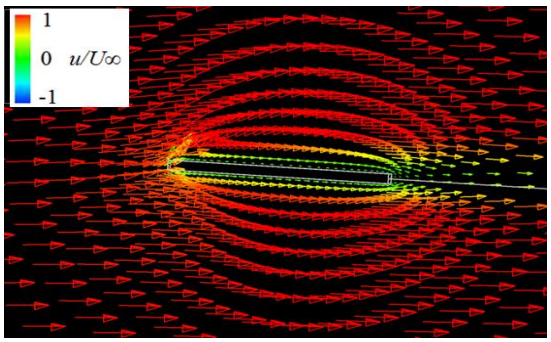

(a) At $\alpha = 4$ deg. $1.0U_\infty$

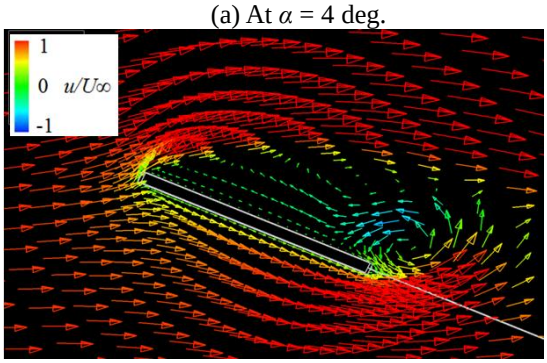

(a) At $\alpha = 24$ deg. $1.0U_\infty$

Figure 8. Velocity vectors for FP with $s/c = 1.0$ at $Re = 4.0\times10^2$ by computation. The colour of each velocity vectors denotes the value of x-component velocity u as shown by the legend on the upper left hand.

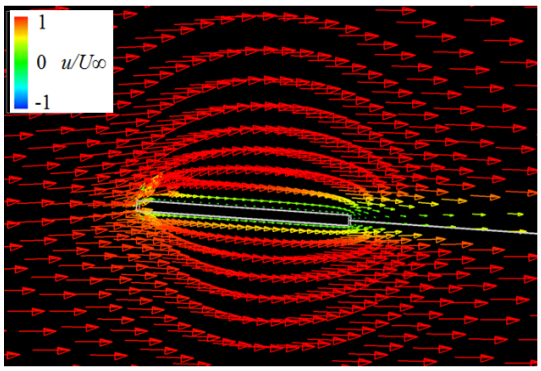

(a) At $\alpha = 4$ deg. $1.0U_\infty$

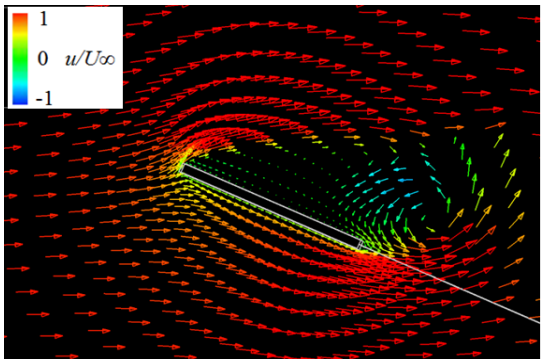

(a) At $\alpha = 24$ deg. $1.0U_\infty$

Figure 9. Velocity vectors for FP with $s/c = 1.0$ at $Re = 8.0\times10^2$ by computation. The colour of each velocity vectors denotes the value of x-component velocity u as shown by the legend on the upper left hand.

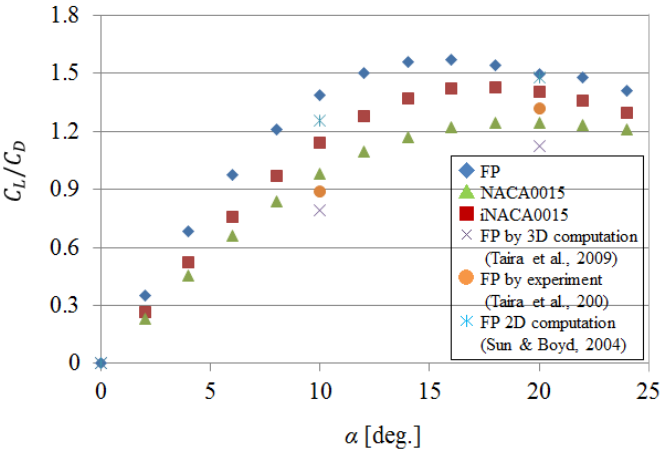

Figure 10. Aerodynamic characteristics: lift-to-drag ratio C_L/C_D versus attack angle α at $Re = 1.0\times10^2$. ×, 3D computation by Taira et al. [21] (for FP with $AR = 2$ and $t/c = 0.037$ at $Re = 1.0\times10^2$ with a grid size of 200×88×128). ●, Experiment by Taira et al. [21] (for FP with $AR = 2$ and $t/c = 0.037$ at $Re = 1.0\times10^2$). ×, 2D computation by Sun & Boyd [15] (for FP with $t/c = 0.05$ at $Re = 1.357\times10^2$ and $Ma = 0.2$).

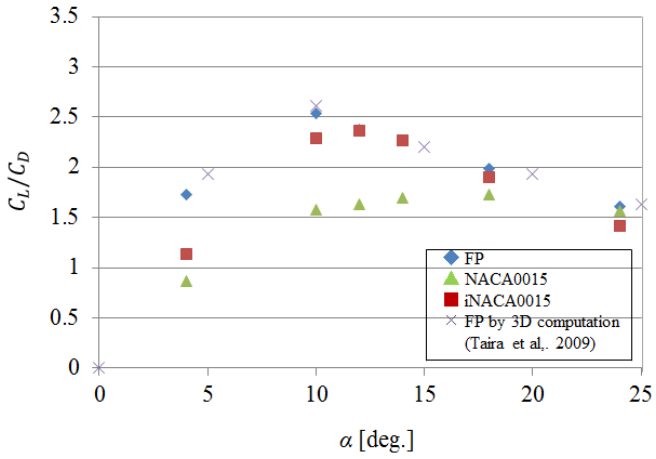

Figure 11. Aerodynamic characteristics: lift-to-drag ratio C_L/C_D versus attack angle α at $Re = 4.0\times10^2$. × , 3D computation by Taira et al. [21] (for FP with $AR = 2$ and $t/c = 0.037$ at $Re = 3.0\times10^2$ with a grid size of 200×88×128).

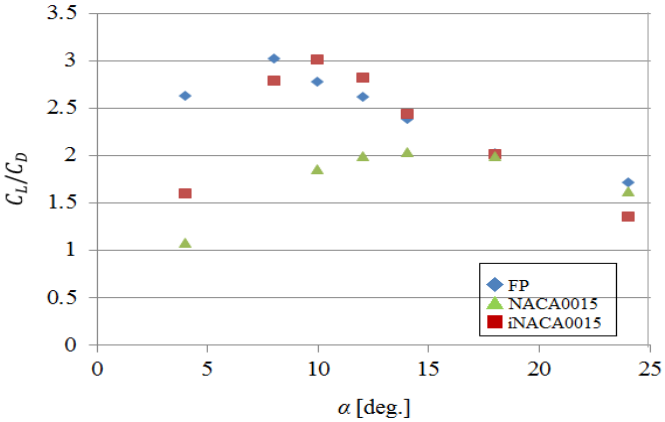

Figure 12. Aerodynamic characteristics: lift-to-drag ratio C_L/C_D versus attack angle α at $Re = 8.0\times10^2$.

Influence of Cross-sectional geometry upon flow

For the other airfoils, it is possible for the flow to be classified into the three groups in the ranges of $Re = 1.0\times10^2 - 8.0\times10^2$ and $\alpha = 4$ - 24 deg. Fig. 15 summaries the results. That is, the figure denotes the stability diagram on the Re- α plane. Panels (a), (b) and (c) are for FP, NACA0015 and iNACA0015, respectively.

First, we look at FP (Fig. 15(a)). As Re or α increases, the flow becomes from the group(1) to the group(2) and finally to the group(3); namely, from steady to unsteady and from two-dimensional to three-dimensional. This transitional feature is the same for NACA0015 (Fig. 15(b)) and iNACA0015 (Fig. 15(c)). To be strict, panel,(a) and (c) coincide with each other, and are slightly different from panel (b). We can confirm this from the comparison among Figs.10 – 12, qualitatively and quantitatively.

The similarity between FP and iNACA0015 could suggest the importance of shape leading edges of airfoils. In other words, in this Re region, it is considered that the airfoil's geometry with a sharp leading edges contributes to the improvement aerodynamic.

Next we look at the transition from steady to unsteady. If we remind the maximum C_L/C_D shown in Fig. 10 - 12., the boundary of transition can be seen to correspond to the maximum value of C_L/C_D.

Appendix: the effect of span upon computation

In computation, we assume the periodic boundary condition at both the ends model's span. Fig. 16 shows Iso-Q surfaces with $QC^2/U_\infty^2 = 3.0$ by computation for NACA0015 at $Re = 8.0\times10^2$ and $\alpha = 18$ deg. The colour of the surfaces denotes the value of relative helicity H_R as shown by the legend on the upper right hand. Panels (a) –(b) are almost the same with each other. Then, we can see that s is enough long for accurate computation.

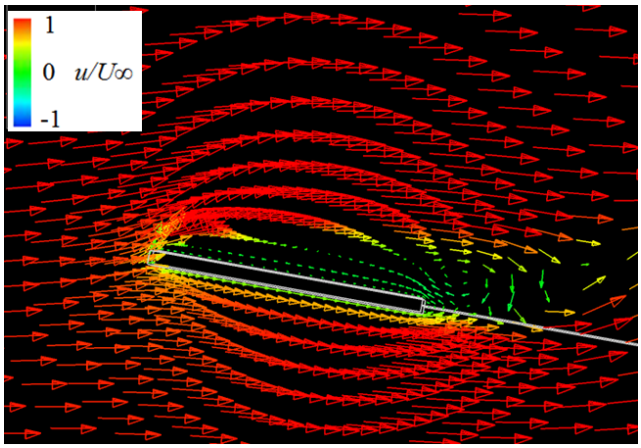

Figure 13. Velocity vectors for FP with $s/c = 1.0$ at $Re = 8.0\times10^2$ and $\alpha = 10$ deg. by computation. The colour of each velocity vectors denotes the value of x-component velocity u as shown by the legend on the upper left hand.

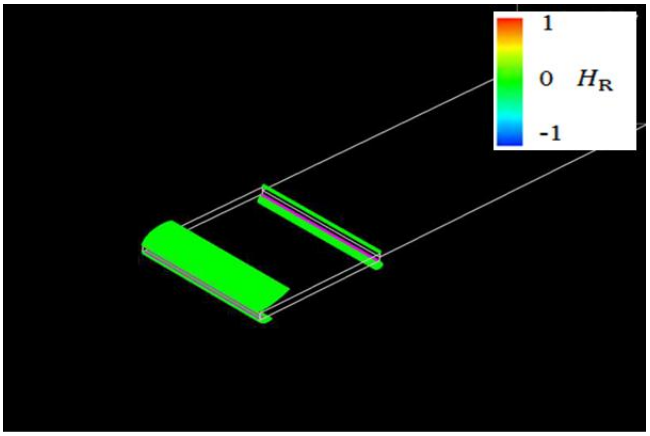

(a) At α = 4 deg.

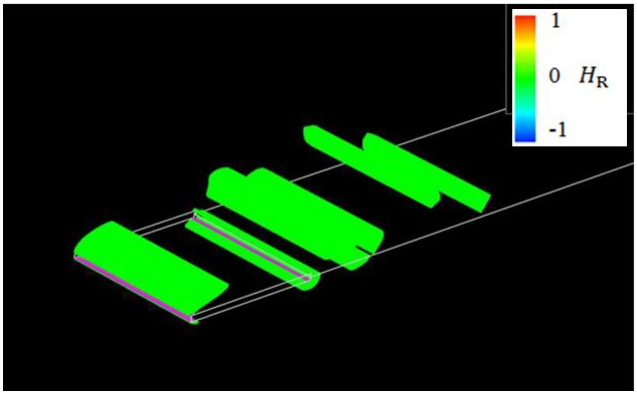

(b) At α = 10 deg.

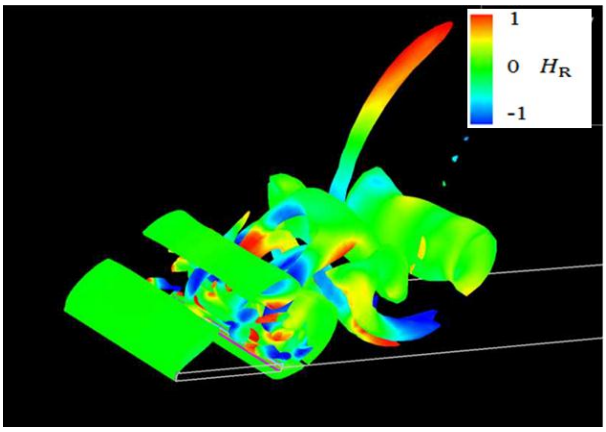

(c) At α = 24 deg.

Figure 14. Iso-Q surfaces with $QC^2/U_\infty{}^2$ = 3.0 by computation for FP with s/c = 1.0 at Re = 8.0×10^2 and α = 4 – 24 deg. The colour of the surfaces denotes the value of relative helicity H_R as shown by the legend on the upper right hand.

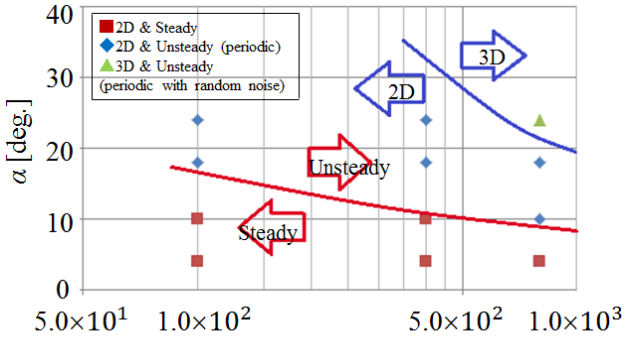

(a) For FP

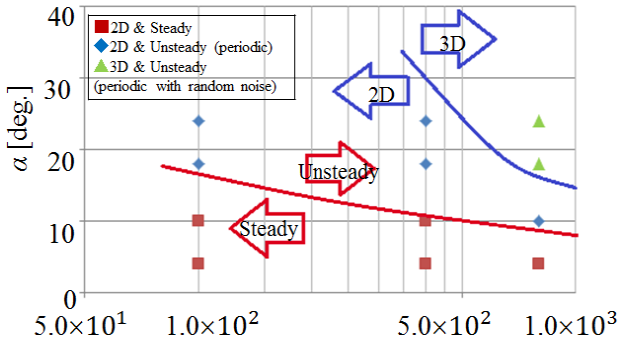

(b) For NACA0015

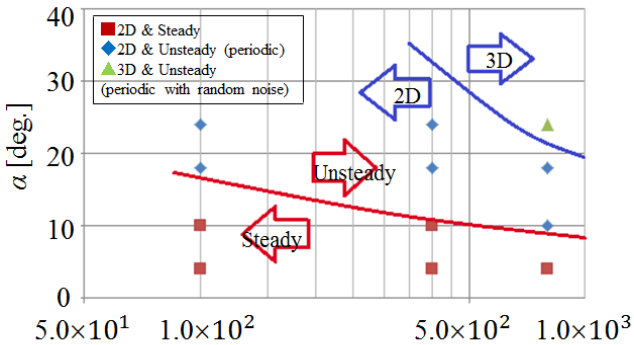

(c) For iNACA0015

Fig.15 Stability diagram on the Re-α plane. ■, Two-dimensional and steady; ◆, two-dimensional and unsteady (periodic); ▲, three-dimensional and unsteady (periodic with random noise).

CONCLUSION

We have investigated the relationship between various aerodynamic characteristics and attack angle α for flat plate, NACA0015 and iNACA0015 (the NACA0015 placed back to front) by numerical analysis and water – tank experiment at Re = 1.0×10^2 – 8.0×10^2. Then, we investigate the effects of attack angle α upon various aerodynamic characteristics such as the lift coefficient C_L, drag coefficient C_D and the lift-to-drag ratio C_L/C_D. In order to discuss the revealed α effects, we visualise the flow around the airfoils using the Q value, the helicity, streamlines distributions around the airfoils at α = 0 – 24 deg., together with PIV analysis based on water – tank experiment. The main results are as follows (1)The velocity vector obtained from the experimental results matches the streamline obtained by numerical analysis.(2)At Re = 1.0×10^2 – 8.0×10^2, the flat plate always showed excellent aerodynamic characteristics. In addition, wing with a sharp leading edge such as FP and iNACA0015 show good wing characteristics in low Reynolds number region.(3)The attack angle at which the lift to drag ratio attains the maximum corresponds to the transition from steady state to unsteady (periodic) state. (4)FP is similar not with NACA0015 but with iNACA0015 from an aerodynamic point of view.

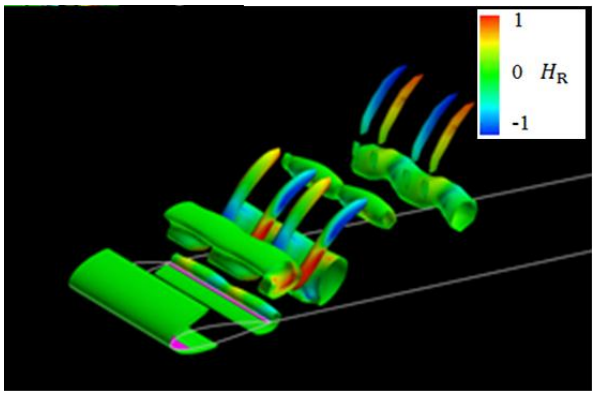

(a)With s/c = 1.0

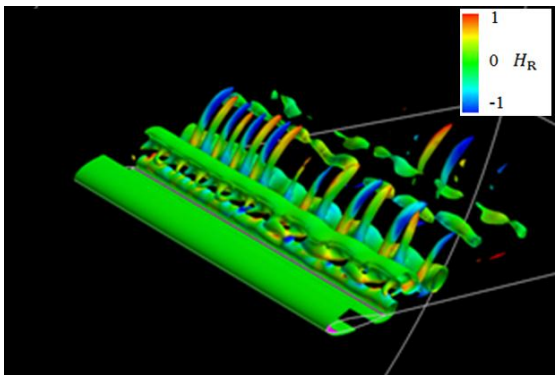

(b)With s/c = 3.9

Figure 16. Iso-Q surfaces with $QC^2/U_\infty{}^2$ = 3.0 by computation for NACA0015 at Re = 8.0×10^2 and α = 18 deg. The colour of the surfaces denotes the value of relative helicity H_R as shown by the legend on the upper right hand.

REFERENCES

(1) Jacobs, E. N. and Sherman, A., "Airfoil Section Characteristics as Affected by Variations in the Reynolds Number," NACA Technical Report, No. 586, pp. 227 – 267, 1937.
(2) Abbott, I. H. and Doenhoff, A. E. von., Theory of Wing Sections, Dover, New York, pp. 462 – 463, 1958.
(3) Riegels, F. W., Aerofoil Sections, Butterworths, London, 1961.
(4) Eppler, R., Airfoil Design and Data, Springer-Verlag, Berlin, 1990.
(5) Kawano, H., "Three-Dimensional Obstacle Avoidance of Blimp-Type Unmanned Aerial Vehicle Flying in Unknown and Non-Uniform Wind Disturbance," Journal of Robotics and Mechatronics, Vol. 19, No. 2, pp. 166 – 173, 2007.
(6) Iwata, K., Matsubara, K., Kawasaki, K. and Matsumoto, O., "Turbojet Engine for Aerial Cargo Robot (ACR)," Journal of Robotics and Mechatronics, Vol. 24, No. 6, pp. 1040 – 1045, 2012.
(7) McMasters, J. H. and Henderson, M. L., "Low Speed Single Element Airfoil Synthesis," Tech. Soaring, Vol. 6, pp. 1 – 21, 1980.
(8) Okamoto, M. Yasuda, K. and Azuma, A., "Aerodynamic Characteristics of the Wings and Body of a Dragonfly," Journal of Experimental Biology, Vol. 199, pp. 281 – 294, 1996.
(9) Abe, H., Tutui, Y. and Yoshiki, H., "Aerodynamic Characteristics of an Airfoil in Turbulent and Low-Reynolds-Number Flows: Experiments with a Jet Grid," Transactions of the Japan Society of Mechanical Engineers Series B, Vol. 62 , No. 602, pp. 3592 – 3598, 1996 (in Japanese).
(10) Sunada, S., Sakaguchi, A. and Kawachi, K., "Airfoil Section Characteristics at a Low Reynolds Number," Transactions ASME, Journal of Fluids Engineering, Vol. 199, pp. 129 – 135, 1997.
(11) Abe, H. "Aerodynamic Characteristics of an Airfoil in Turbulent and Low-Reynolds-Number Flows," Technical Report of Mechanical Engineering Laboratory, AIST, Vol. 186, 2000 (in Japanese).
(12) Isikawa, H., Kudo, D., Kiya, M., Mochizuki, O. and Zheng, Z., "Aerodynamic Characteristics of a Flat-Plate Wing with Leading-Edge Serrations," Transactions of the Japan Society of Mechanical Engineers, Series B, Vol. 67, No. 655, pp. 680 – 687, 2001 (in Japanese).
(13) Motohashi, T., "Characteristics of Rectangular Wings at Low Reynolds Numbers," Proc. 39th Aircraft Symposium, JSASS, Paper No. 3D6, pp. 1 – 4, 2001 (in Japanese).
(14) Nakane, N. Tanaka.T. and Motohashi, T., "Aerodynamic Characteristics of NACA0012 in a Wide Reynolds Number range," Proc. 35th Fluid Dynamics Conference, JSASS, pp. 179 – 182, 2003 (in Japanese).
(15) Sun, Q. and Boyd, I. D., "Flat-Plate Aerodynamics at Very Low Reynolds Number," Journal of Fluid Mechanics, Vol. 502, pp. 199 – 206, 2004.

(16) Takagi, R., "Aerodynamic Characteristics of NACA4402 in Low Reynolds Number Flows," Journal of the Japan Society for Aeronautical and Space Sciences, Vol. 54, No. 631 pp. 367 – 373, 2006 (in Japanese).
(17) Ohtake, T., Nakae, Y. and Motohashi, T., Journal of the Japan Society for Aeronautical and Space Sciences, Vol. 55, pp. 439 – 445, 2007 (in Japanene).
(18) Yagi, H. and Kawahara, M., "Optimal Shape Determination of a Body Located in Incompressible Viscous Fluid Flow," Computer Methods in Applied Mechanical and Engineering, Vol. 196, pp. 5084 – 5091, 2007.
(19) Katamine, E., Nishihashi, N. and Azegami, H., "Shape Optimization of Steady-State Viscous Flow Fields for Drag Minimization and Lift Maximization," Transactions of the Japan Society of Mechanical Engineers, Series B, Vol. 74, No. 748, pp. 2426 – 2433, 2008 (in Japanese).
(20) Ohtake, T. and Motohashi, T., "Flow Field around NACA0012 Airfoil at Low Reynolds Numbers," Journal of the Japan Society for Aeronautical and Space Sciences, Vol. 57, pp. 397 – 404, 2009 (in Japanene).
(21) Taira, K. and Colonius, T., "Three-Dimensional Flows Around Low-Aspect-Ratio Flat-Plate Wings at Low Reynolds Numbers," Journal of Fluid Mechanics, Vol. 623, pp. 187 – 207, 2009.
(22) Hirata, K., Kawakita, M., Iijima, T., Koga, M., Kihira, M. and Funaki, J., "Numerical and Experimental Study on Aerodynamic Characteristics of Basic Airfoils at Low Reynolds Numbers," Journal of Fluid Science and Technology, Vol. 5, pp. 447 – 463, 2010.
(23) Zhou, Y., Md. Mahbub Alam, Yang, H. X., Guo, H. and Wood, D. H., "Fluid Forces on a Very Low Reynolds Number Airfoil and Their Prediction," International Journal of Heat and Fluid Flow, Vol. 32, pp. 329 – 339, 2011.
(24) Ebata, S., Yasuda, T., Minagawa, H., Miyamoto, Y. and Satofuka, N., "A Study of Cross-Sectional Shape of Wing for Underwater Glider at Low Reynolds Number Region," Transactions of the Japan Society of Mechanical Engineers, Series B, Vol. 79, No. 806, pp. 12 – 25, 2013 (in Japanene).
(25) Suzuki, K., Minami, K. and Inamuro, T., "Lift and Thrust Generation by a Butterly-Like Flapping Wing-Body Model: Immersed Boundary-Lattice Boltzmann Simulations," *Journal of Fluid Mechanics*, Vol. 767 (2015), pp. 659 – 695.
(26) Hirata, K., Nozawa, R., Kondo, S., Onishi, K. and Tanigawa, H., "On High-Performance Airfoil at Very Low Reynolds Number," *Journal of Robotics and Mechatronics*, Vol. 28, No. 3 (2016), pp. 273 – 285.